

**Angle-dependent magic wavelengths for the  $4s_{1/2} \rightarrow 3d_{5/2,3/2}$  transitions of  $\text{Ca}^+$  ions**

Jun Jiang,\* Li Jiang, Z. W. Wu, Deng-Hong Zhang, Lu-You Xie, and Chen-Zhong Dong

*Key Laboratory of Atomic and Molecular Physics and Functional Materials of Gansu Province, College of Physics and Electronic Engineering, Northwest Normal University, Lanzhou 730070, People's Republic of China*

(Received 25 January 2019; published 22 March 2019)

The dynamic polarizabilities of the atomic states with angular momentum  $j > 1/2$  are sensitive to the angle between the quantization axis  $\hat{e}_z$  and the polarization vector  $\hat{e}$  owing to the contribution of anisotropic tensor polarizabilities. The magic wavelength at which the differential Stark shift of an atomic transition nullifies depends on this angle. We identified the magic wavelengths for the  $4s_{1/2} \rightarrow 3d_{3/2,5/2}$  transitions of  $\text{Ca}^+$  ions at different angles between  $\hat{e}_z$  and  $\hat{e}$  in the case of linearly polarized light. The magic wavelengths near 395.79 nm, which lie between the  $4s_{1/2} \rightarrow 4p_{1/2}$  and  $4s_{1/2} \rightarrow 4p_{3/2}$  transition wavelengths, remain insensitive to the angle, while the longest magic wavelength, which is around 1000 nm, for each of the magnetic sublevel transitions is very sensitive to the angle. We suggest that accurate measurements on the longest magic wavelengths for the  $4s_{1/2} \rightarrow 3d_{5/2}$  and  $4s_{1/2} \rightarrow 3d_{3/2}$  transitions can be used to determine the oscillator strengths for the  $4s_{1/2} \rightarrow 4p_{1/2,3/2}$ ,  $3d_{5/2} \rightarrow 4p_{3/2}$ , and  $3d_{3/2} \rightarrow 4p_{1/2,3/2}$  transitions, and the difference of the static polarizabilities of the  $4s_{1/2}$  and  $3d_{5/2}$  states, and the tensor polarizability of the  $3d_{5/2}$  state.

DOI: [10.1103/PhysRevA.99.032510](https://doi.org/10.1103/PhysRevA.99.032510)**I. INTRODUCTION**

Techniques involving laser cooling and trapping of neutral atoms or ions have a lot of applications in quantum information [1–4], and in high-precision frequency and spectroscopy measurements [5–12]. However, the laser field can cause Stark shifts of atomic energy levels and transitions. The problem of eliminating the Stark shifts for a given transition can be solved by trapping an atom or ion at magic wavelengths at which the Stark shifts of both the upper and lower states are the same and the shifts of the transition frequency vanish [13,14]. Also, the systematic uncertainties of high-precision measurement can be reduced by optical traps at the magic wavelengths [15,16]. In order to theoretically determine the magic wavelength of an atomic transition, accurate dynamic polarizabilities are required for the relevant atomic states, which consist of isotropic scalar and anisotropic vector and tensor parts [16–18]. The anisotropic parts resulting in the light shift depend on not only on the angular momentum projection  $m$  but also the angle between the quantization axis  $\hat{e}_z$  and the electric polarization vector  $\hat{e}$  of the laser. This will make accurate determinations of the magic wavelengths much more difficult in experiments.

Due to the simple energy-level structure and the long lifetime of the  $3d_{5/2}$  state, calcium ions have been chosen as one of the candidates for optical frequency standard [19–26]. In a recent experiment with a radio-frequency Paul trap, the accuracy of  $^{40}\text{Ca}^+$  optical clocks has achieved a level of  $3.4 \times 10^{-17}$  [12]. In this experiment, excess micromotion was identified as the biggest factor affecting the accuracy of the  $^{40}\text{Ca}^+$  clock [12]. If the weak micromotions of trapped ions can be handled with more accuracy, such kinds of  $^{40}\text{Ca}^+$

clocks could achieve a systematic fractional uncertainty of about  $10^{-18}$ . Therefore, all-optical magic trapping of  $\text{Ca}^+$  ions is worth being tried for diminishing substantially the micromotion-induced shifts [12,15]. The magic wavelengths of  $\text{Ca}^+$  ions have been studied both in theories and experiments [15,27,28]. Two magic wavelengths of the  $^{40}\text{Ca}^+$   $4s \rightarrow 3d_{5/2}(m = 1/2, 3/2)$  clock transitions near 395.79 nm for linearly polarized light have been measured with very high accuracy and they agree with all existing theoretical results very well [15,27,28]. However, these magic wavelengths are very close to the  $4s_{1/2} \rightarrow 4p_{3/2}$  and  $4s_{1/2} \rightarrow 4p_{1/2}$  resonant transition wavelengths of 393.366 and 396.847 nm. Therefore, they are not good for the use of magic trapping, as the near-resonant light has high photon spontaneous scattering rates which result in a high heating process [29,30].

Another important application of magic wavelengths and magic-zero wavelengths, at which the dynamic polarizability is zero, is to test the atomic structure and determine atomic parameters [31–37]. For example, the ratio of  $^{87}\text{Rb}$  D-line dipole matrix elements was determined with an accuracy up to 15 ppm by using the high-precision measurement of the magic-zero wavelength [32]. The accuracy of atomic transition matrix elements can arrive at the  $10^{-3}$  level by the measurement of the ac Stark shift around magic-zero wavelength [31]. Measurement of the two magic wavelengths at 395.7992(7) and 395.7990(7) nm of the  $\text{Ca}^+$  clock transition determined the ratio of the oscillator strengths for the  $4s_{1/2} \rightarrow 4p_{3/2}$  and  $4s_{1/2} \rightarrow 4p_{1/2}$  transitions as 2.027(5) [15].

In this manuscript, the variations of the magic wavelengths with the applied laser direction are determined in detail. Moreover, we suggest that the oscillator strengths for the  $4s_{1/2} \rightarrow 4p_{1/2,3/2}$ ,  $3d_{5/2} \rightarrow 4p_{3/2}$ , and  $3d_{3/2} \rightarrow 4p_{1/2,3/2}$  transitions, the difference of the static polarizabilities of the  $4s_{1/2}$  and  $3d_{5/2}$  states, and the tensor polarizability of the  $3d_{5/2}$  state can be determined by measuring the longest magic wavelengths

\*phyjiang@yeah.net

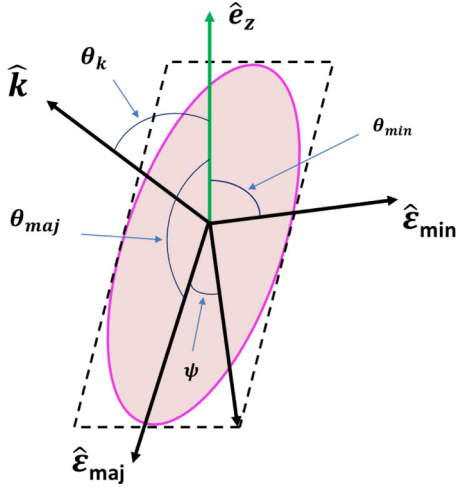


FIG. 1. Representation of the electromagnetic plane-wave geometrical parameters. The surface represents the ellipse swept out by the electric field vector in one period. The unit vector  $\hat{\epsilon}_{\text{maj}}(\hat{\epsilon}_{\text{min}})$  aligns with the semimajor (-minor) axis of the ellipse.  $\hat{e}_z$  is the quantization axis, which selects the direction of the magnetic field in the experiment.  $\hat{k}$  represents the direction of the wave vector.  $\theta_k$  is the angle between  $\hat{e}_z$  and  $\hat{k}$ . The parameters  $\hat{\epsilon}_{\text{maj}}$ ,  $\hat{\epsilon}_{\text{min}}$ , and  $\hat{k}$  are mutually orthogonal.  $\theta_{\text{maj}}$  ( $\theta_{\text{min}}$ ) is the angle between  $\hat{\epsilon}_{\text{maj}}$  ( $\hat{\epsilon}_{\text{min}}$ ) and  $\hat{e}_z$ .  $\psi$  is directly related to the degree of circular polarization.

for the  $4s_{1/2} \rightarrow 3d_{3/2,5/2}$  transitions. Finally, a brief summary is given in Sec. IV. Atomic units,  $\hbar = m = |e| = 1$ , are used throughout this paper unless stated otherwise.

## II. THEORY

The necessary atomic parameters of  $\text{Ca}^+$  ions such as energy levels, matrix elements, and polarizabilities have been calculated using the relativistic configuration interaction with the core polarization (RCICP) approach [38] in our previous work [39]. These data are not repeated here for the sake of brevity.

For a polarized light, the dynamic polarizability of an atomic state  $i$  is given by [17,18,40]

$$\alpha_i(\omega) = \alpha_i^S(\omega) + \mathcal{A} \cos \theta_k \frac{m_{j_i}}{2j_i} \alpha_i^V(\omega) + \frac{3 \cos^2 \theta_p - 1}{2} \frac{3m_{j_i}^2 - j_i(j_i + 1)}{j_i(2j_i - 1)} \alpha_i^T(\omega), \quad (1)$$

where  $\alpha_i^S(\omega)$ ,  $\alpha_i^V(\omega)$ ,  $\alpha_i^T(\omega)$  represent the scalar, vector, and tensor polarizabilities as given in Refs. [17,18,40], respectively.  $m_{j_i}$  is the component of total angular momentum  $j_i$ . There are no tensor polarizabilities for the states with  $j \leq 1/2$ .  $\theta_k$  is the angle between the wave vector  $\hat{k}$  and the quantization axis  $\hat{e}_z$ ,  $\cos \theta_k = \hat{k} \cdot \hat{e}_z$ . The relevant diagram is shown in Fig. 1. The  $\theta_p$  relates to the polarization vector  $\hat{e}$  and the  $\hat{e}_z$  axis. For a more general geometrical interpretation of  $\theta_p$ , it is useful to further introduce the parameters  $\theta_{\text{maj}}$ ,  $\theta_{\text{min}}$ , and  $\psi$ .  $\cos^2 \theta_p$  can be written in the form [18]

$$\cos^2 \theta_p = \cos^2 \psi \cos^2 \theta_{\text{maj}} + \sin^2 \psi \cos^2 \theta_{\text{min}}, \quad (2)$$

where the parameter  $\theta_{\text{maj}}$  ( $\theta_{\text{min}}$ ) is the angle between the major (minor) axis of the ellipse and the  $\hat{e}_z$  axis. From a geometrical consideration,  $\theta_k$  and  $\theta_p$  satisfy the relation  $\cos^2 \theta_k + \cos^2 \theta_p \leq 1$  [17,40]. The angle  $\psi$  is directly related to the degree of polarization of light.  $\mathcal{A}$  represents the degree of polarization, which is given by

$$\mathcal{A} = \sin 2\psi. \quad (3)$$

In particular,  $\mathcal{A} = 0$  corresponds to linear polarization, while  $\mathcal{A} = +1$  (or  $-1$ ) corresponds to right- (or left-) circular polarization. In the experiment, however,  $\mathcal{A}$  could not absolutely be equal to zero. In this case, the vector polarizability contributes to the total dynamic polarizability. In order to get rid of the vector part in the experiment, one can set  $\cos \theta_k$  equal to zero, i.e.,  $\hat{e}_z \perp \hat{k}$ .

In the case of  $\cos \theta_k = 0$ , the quantization axis  $\hat{e}_z$  is perpendicular to the wave vector  $\hat{k}$ , and the angle between the direction of polarization and  $\hat{e}_z$  varies in the plane of polarization. When  $\mathcal{A} = 0$  or  $\cos \theta_k = 0$ , the dynamic polarizability can be easily simplified from Eq. (1) as follows:

$$\alpha_i(\omega) = \alpha_i^S(\omega) + \frac{3 \cos^2 \theta_p - 1}{2} \frac{3m_{j_i}^2 - j_i(j_i + 1)}{j_i(2j_i - 1)} \alpha_i^T(\omega). \quad (4)$$

The dynamic polarizability depends on not only the value of  $m$  but also the  $\theta_p$  in a certain frequency  $\omega$ .

In the case of  $\cos \theta_k = 0$ , parameters  $\theta_{\text{maj}}$  and  $\theta_{\text{min}}$  satisfy the relation

$$\theta_{\text{maj}} + \theta_{\text{min}} = \frac{\pi}{2}. \quad (5)$$

With the use of Eqs. (3) and (5), Eq. (2) can be further simplified to

$$\cos^2 \theta_p = \frac{1}{2} + \frac{\sqrt{1 - \mathcal{A}^2}}{2} \cos 2\theta_{\text{maj}}. \quad (6)$$

Therefore, for a given value of  $\mathcal{A}$ ,  $\cos^2 \theta_p$  satisfies

$$\frac{1}{2} - \frac{\sqrt{1 - \mathcal{A}^2}}{2} \leq \cos^2 \theta_p \leq \frac{1}{2} + \frac{\sqrt{1 - \mathcal{A}^2}}{2}. \quad (7)$$

As seen from Eq. (7),  $\mathcal{A} = 0$  corresponds to  $0 \leq \cos^2 \theta_p \leq 1$ , in which  $\cos^2 \theta_p$  covers the largest range  $[0,1]$ , while  $|\mathcal{A}| = 1$  just gives rise to  $\cos^2 \theta_p = 1/2$ . In the following part, we mainly discuss the case of linearly polarized light with  $\cos \theta_k = 0$  and  $0 \leq \cos^2 \theta_p \leq 1$ .

## III. RESULTS AND DISCUSSION

### A. Magic wavelengths for the $4s_{1/2} \rightarrow 3d_{5/2}$ transition

First, two particular cases are considered. One of them is  $\cos^2 \theta_p = 1$ . This means the  $\hat{e}_z$  axis is perpendicular to the wave vector but parallel to the polarization vector, i.e.,  $\hat{e}_z \perp \hat{k}$  and  $\hat{e}_z \parallel \hat{e}$ . In this case, Eq. (4) becomes

$$\alpha_i(\omega) = \alpha_i^S(\omega) + \frac{3m_{j_i}^2 - j_i(j_i + 1)}{j_i(2j_i - 1)} \alpha_i^T(\omega). \quad (8)$$

Another case is  $\cos^2 \theta_p = 0$ , which means the  $\hat{e}_z$  axis is perpendicular to the wave vector and the polarization vector,

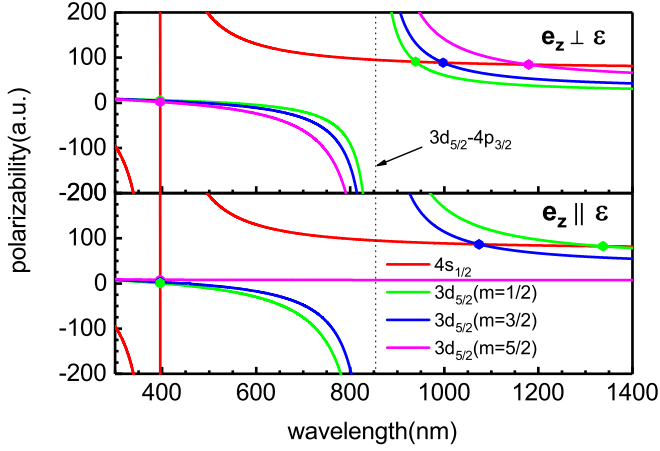


FIG. 2. Dynamic polarizabilities (in a.u.) of the  $4s$  and  $3d_{5/2}(m = 1/2, 3/2, 5/2)$  states in the wavelength range 300–1400 nm. The upper panel plots the dynamic polarizabilities in the case of  $\hat{e}_z \perp \hat{\epsilon}$ . The lower panel plots the dynamic polarizabilities in the case of  $\hat{e}_z \parallel \hat{\epsilon}$ . The approximate position of the  $3d_{5/2} \rightarrow 4p_{3/2}$  resonance is indicated by the vertical dotted line.

i.e.,  $\hat{e}_z \perp \hat{k}$  and  $\hat{e}_z \perp \hat{\epsilon}$ . Equation (4) is simplified as follows:

$$\alpha_i(\omega) = \alpha_i^S(\omega) - \frac{3m_j^2 - j_i(j_i + 1)}{2j_i(2j_i - 1)} \alpha_i^T(\omega). \quad (9)$$

Figure 2 shows the dynamic polarizabilities of the  $4s$  and  $3d_{5/2}$  states in the wavelength range 300–1400 nm for the laser polarization direction perpendicular (upper panel) and parallel (lower panel) to the quantization axis, respectively. Since the dynamic polarizability of the  $4s_{1/2}$  state has only the isotropic scalar part, the dynamic polarizability of the  $4s_{1/2}$  state in the case of  $\hat{e}_z \perp \hat{\epsilon}$  is the same as the one in  $\hat{e}_z \parallel \hat{\epsilon}$ . However, the dynamic polarizabilities of the  $3d_{5/2}$  state for both cases  $\hat{e}_z \perp \hat{\epsilon}$  and  $\hat{e}_z \parallel \hat{\epsilon}$  are completely different for each of the magnetic components due to the contribution from the anisotropic tensor part. For example, when the wavelength is close to the  $3d_{5/2} \rightarrow 4p_{3/2}$  resonant transition wavelength (854.21 nm), the dynamic polarizability of the  $3d_{5/2}(m = 5/2)$  state is infinite in the case of  $\hat{e}_z \perp \hat{\epsilon}$  but it is finite in  $\hat{e}_z \parallel \hat{\epsilon}$ . To be more specific, as per the explanation in Ref. [39], the contributions of the tensor and scalar terms from the  $3d_{5/2} \rightarrow 4p_{3/2}$  transition cancel each other out in the case of  $\hat{e}_z \parallel \hat{\epsilon}$ . The intersections of the dynamic polarizabilities of  $4s_{1/2}$  and each magnetic state of  $3d_{5/2}$  give rise to magic wavelengths. For a given magnetic sublevel transition, we can see the magic wavelengths are different for the cases  $\hat{e}_z \perp \hat{\epsilon}$  and  $\hat{e}_z \parallel \hat{\epsilon}$ . Two magic wavelengths have been found for each of the  $4s \rightarrow 3d_{5/2}$  magnetic transitions [except that the  $4s \rightarrow 3d_{5/2}(m = 5/2)$  transition with  $\hat{e}_z \parallel \hat{\epsilon}$  has only one magic wavelength]—one lies between the  $4s_{1/2} \rightarrow 4p_{1/2,3/2}$  transition wavelengths, and the other is the longest magic wavelength, longer than the  $4p_{3/2} \rightarrow 3d_{5/2}$  transition wavelength (854.21 nm).

Furthermore, we investigate the variation of the magic wavelengths for the  $4s \rightarrow 3d_{5/2}$  transition with  $\cos^2 \theta_p$ . Figure 3 shows the dependence of the magic wavelengths near 395.79 nm upon  $\cos^2 \theta_p$ , which lie between the  $4s_{1/2} \rightarrow 4p_{1/2}$  and  $4s_{1/2} \rightarrow 4p_{3/2}$  transition wavelengths. As shown

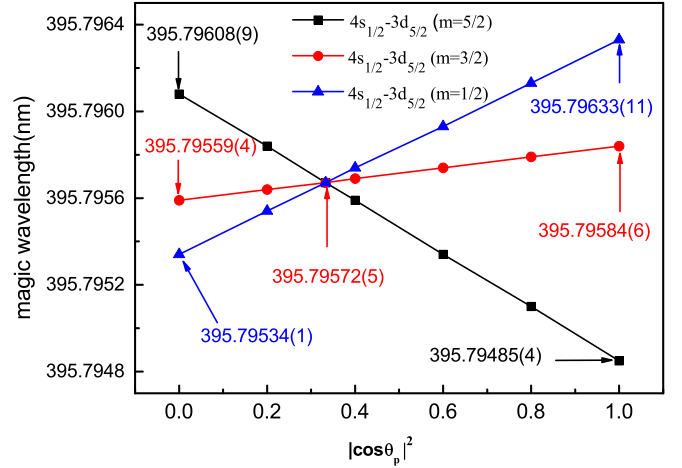


FIG. 3. The dependence of magic wavelengths, which lie between the  $4s_{1/2} \rightarrow 4p_{1/2}$  transition wavelength (393.37 nm) and  $4s_{1/2} \rightarrow 4p_{3/2}$  transition wavelength (396.85 nm), of each magnetic sublevel transition of  $4s_{1/2} \rightarrow 3d_{5/2}$  upon  $\cos^2 \theta_p$  in the case of linearly polarized light.

clearly from the Fig. 3, the magic wavelengths change nearly linearly with  $\cos^2 \theta_p$ . Also, the difference of magic wavelengths is small for different magnetic sublevel transitions. Meanwhile, the magic wavelengths of each magnetic transition change weakly with  $\cos^2 \theta_p$  as well. For example, for the  $4s_{1/2} \rightarrow 3d_{5/2}(m = 5/2)$  transition, the difference in magic wavelengths is just 0.0012 nm for  $\cos^2 \theta_p = 0$  and  $\cos^2 \theta_p = 1$ . The absolute values of derivatives of magic wavelengths for the  $4s_{1/2} \rightarrow 3d_{5/2}(m = 1/2, 3/2, 5/2)$  transitions,  $|d\lambda_{\text{magic}}/d\cos^2 \theta_p|$ , are 0.00099, 0.00025, 0.0012, respectively, which means that these magic wavelengths are not sensitive to the quantity  $\cos^2 \theta_p$ .

Figure 4 shows the  $\cos^2 \theta_p$  dependence of the longest magic wavelengths for the  $4s_{1/2} \rightarrow 3d_{5/2}$  transition. As seen from Fig. 4, the magic wavelengths for the  $4s_{1/2} \rightarrow 3d_{5/2}(m = 1/2, 3/2)$  transitions become longer with the

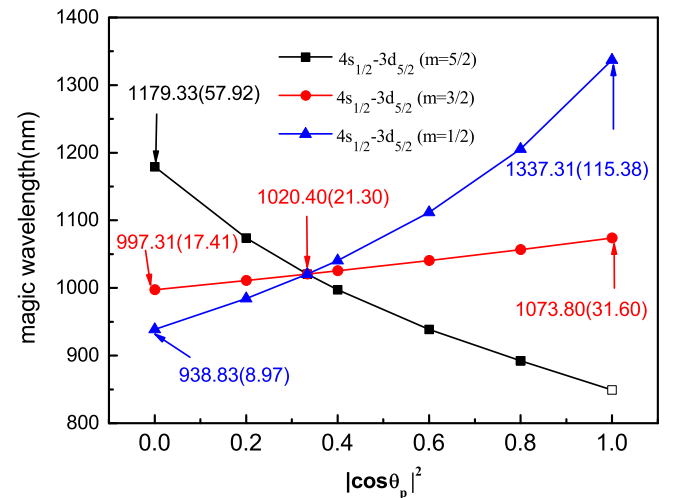


FIG. 4. Same as Fig. 3 but for magic wavelengths longer than the  $3d_{5/2} \rightarrow 4p_{3/2}$  transition wavelength (854.21 nm).

TABLE I. The contributions of individual transitions to the polarizabilities (in a.u.) of the  $4s_{1/2}$  and  $3d_{5/2}(m = 1/2)$  states at the magic wavelengths for the different  $\cos^2\theta_p$ . The contribution to the polarizability of the  $4s_{1/2}$  state from all other transitions (excluding the  $4s_{1/2} \rightarrow 4p_{1/2,3/2}$  transitions) is noted as “Rest”. The contribution to polarizability of the  $3d_{5/2}$  state from all other transitions (excluding the  $3d_{5/2} \rightarrow 4p_{3/2}$  transition) is noted as “Rest”.

| $\cos^2\theta_p$ | 0          | 0.2        | 0.4                 | 0.6        | 0.8        | 1.0        |
|------------------|------------|------------|---------------------|------------|------------|------------|
| $\omega$ (a.u.)  | 0.04853208 | 0.04628478 | 0.04378998          | 0.04088149 | 0.03779304 | 0.03407102 |
| $\lambda$ (nm)   | 938.8296   | 984.4132   | 1040.4972           | 1111.6229  | 1205.6017  | 1337.3054  |
|                  |            |            | $4s_{1/2}$          |            |            |            |
| $4p_{1/2}$       | 29.4065    | 29.2935    | 28.9528             | 28.3787    | 27.5610    | 26.4827    |
| $4p_{3/2}$       | 58.1152    | 57.8966    | 57.2372             | 56.1254    | 54.5404    | 52.4473    |
| Rest             | 3.4142     | 3.4141     | 3.4138              | 3.4132     | 3.4124     | 3.4112     |
| Total            | 90.9360    | 90.6043    | 89.6037             | 87.9174    | 78.6890    | 82.3412    |
|                  |            |            | $3d_{5/2}(m = 1/2)$ |            |            |            |
| $4p_{3/2}$       | 82.2143    | 81.7986    | 80.5469             | 78.4443    | 75.4632    | 71.5585    |
| Rest             | 8.7217     | 8.8057     | 9.0569              | 9.4731     | 10.0506    | 10.7828    |
| Total            | 90.9360    | 90.6043    | 89.6037             | 87.9174    | 85.5138    | 82.3412    |

increase of  $\cos^2\theta_p$ , while the magic wavelengths for the  $4s_{1/2} \rightarrow 3d_{5/2}(m = 5/2)$  transition become shorter. Moreover, the magic wavelength of each magnetic sublevel transition changes strongly with  $\cos^2\theta_p$ . For example, for the  $4s_{1/2} \rightarrow 3d_{5/2}(m = 1/2)$  transition, the difference in magic wavelengths is 398 nm for  $\cos^2\theta_p = 0$  and  $\cos^2\theta_p = 1$ . The minimum absolute values of derivatives,  $|d\lambda_{\text{magic}}/d\cos^2\theta_p|$ , for the  $4s_{1/2} \rightarrow 3d_{5/2}(m = 1/2, 3/2, 5/2)$  transitions are 228, 77, and 217, respectively. That means these magic wavelengths that are longer than the  $3d_{5/2} \rightarrow 4p_{3/2}$  transition wavelength vary sensitively with  $\cos^2\theta_p$ .

As shown in Figs. 3 and 4, however, different curves intersect at one point. The magic wavelengths are independent of magnetic sublevels at this intersection, and the contribution of tensor polarizabilities is zero. This condition can be attained when  $\cos^2\theta_p = 1/3$  for linearly polarized light. This angle  $\theta_p$  is referred to as a “magic angle” [41] and is given by

$$\theta_p = \arccos\left(\frac{1}{\sqrt{3}}\right) \approx 54.74^\circ. \quad (10)$$

According to Eq. (7), the determination of the “magic angle” requires the condition  $|A| \leq \frac{2\sqrt{2}}{3}$ . The magic wavelengths corresponding to the magic angle are determined for the  $4s_{1/2} \rightarrow 3d_{5/2}$  transition as shown in Figs. 3 and 4. For instance, at the magic angle, the magic wavelengths are 395.79572(5) and 1024.40(21.30) nm for the  $4s_{1/2} \rightarrow 3d_{5/2}$  transition.

In Table I, we list the contributions from some individual transitions on the polarizabilities of the  $4s_{1/2}$  and  $3d_{5/2}(m = 1/2)$  states at the longest magic wavelengths for the different  $\cos^2\theta_p$ . It can be found that the polarizability of the  $4s_{1/2}$  state is dominated by the  $4s_{1/2} \rightarrow 4p_{1/2}$  and  $4s_{1/2} \rightarrow 4p_{3/2}$  resonant transitions, which contribute more than 96%. The contribution from all other transitions to the polarizability of  $4s_{1/2}$ , noted as “Rest”, is very small and changes slowly with the changes of frequency (or  $\cos^2\theta_p$ ) of the magic wavelength. The main contribution to the polarizability of the  $3d_{5/2}$  state

comes from the  $3d_{5/2} \rightarrow 4p_{3/2}$  transition and is as high as 86%. The contribution from all other transitions to the  $3d_{5/2}$  state, noted as “Rest”, is just about 14% and changes slowly also with the changes in frequency of the magic wavelength.

At the magic wavelength, the total dynamic polarizabilities of the  $4s_{1/2}$  and  $3d_{5/2}$  states are equal, i.e.,

$$\alpha_{4s_{1/2}}(\omega) - \alpha_{3d_{5/2}}(\omega, \cos^2\theta_p) = 0, \quad (11)$$

in which the total dynamic polarizability of the  $4s_{1/2}$  state,  $\alpha_{4s_{1/2}}(\omega)$ , depends only on  $\omega$ , since there is no tensor polarizability for the state with  $j \leq 1/2$ . According to the data in Table I and the definitions of the dynamic polarizability, Eq. (11) can be written as

$$\frac{f_{4s_{1/2} \rightarrow 4p_{1/2}}}{\Delta E_{4s \rightarrow 4p_{1/2}}^2 - \omega^2} + \frac{f_{4s \rightarrow 4p_{3/2}}}{\Delta E_{4s \rightarrow 4p_{3/2}}^2 - \omega^2} - C \frac{f_{3d_{5/2} \rightarrow 4p_{3/2}}}{\Delta E_{3d_{5/2} \rightarrow 4p_{3/2}}^2 - \omega^2} = G(\omega, \cos^2\theta_p), \quad (12)$$

where  $\Delta E_{i \rightarrow j}$  is the transition energy from  $i$  to  $j$  states;  $f_{i \rightarrow j}$  is the oscillator strength of the  $i \rightarrow j$  transition; and  $C$  can be simplified as

$$C = 1 - \frac{(3 \cos^2\theta_p - 1)(12m_{j_i}^2 - 35)}{80}, \quad (13)$$

where  $m_{j_i}$  is magnetic quantum number of the  $3d_{5/2}$  state.

$G(\omega, \cos^2\theta_p)$  can be written as

$$G(\omega, \cos^2\theta_p) = \alpha_{3d_{5/2}}^R(\omega, \cos^2\theta_p) - \alpha_{4s_{1/2}}^R(\omega), \quad (14)$$

where  $\alpha_{4s_{1/2}}^R(\omega)$  represents the dynamic polarizability of the  $4s_{1/2}$  state, excluding the contributions from the  $4s_{1/2} \rightarrow 4p_{1/2}$  and  $4s_{1/2} \rightarrow 4p_{3/2}$  transitions. That is the Rest value for the  $4s_{1/2}$  state in Table I.  $\alpha_{3d_{5/2}}^R(\omega, \cos^2\theta_p)$  represents the dynamic polarizability of the  $3d_{5/2}$  state, excluding the contribution from  $3d_{5/2} \rightarrow 4p_{3/2}$  transition. That is the Rest value for the  $3d_{5/2}$  state in Table I. By using the definitions of polarizability,  $G(\omega, \cos^2\theta_p)$  can also be written as

$$G(\omega, \cos^2\theta_p) = \sum_n \frac{f_{3d_{5/2} \rightarrow nl}}{\Delta E_{3d_{5/2} \rightarrow nl}^2 - \omega^2} + \frac{3 \cos^2\theta_p - 1}{2} \sum_n C_n \frac{f_{3d_{5/2} \rightarrow nl}}{\Delta E_{3d_{5/2} \rightarrow nl}^2 - \omega^2} - \sum_{n=5} \frac{f_{4s_{1/2} \rightarrow np_j}}{\Delta E_{4s_{1/2} \rightarrow np_j}^2 - \omega^2}, \quad (15)$$

TABLE II. Values of parameters  $A_k$  and  $B_k$  for each of the  $4s_{1/2} \rightarrow 3d_{5/2}$  magnetic sublevel transitions.

| Transition                                | $A_0$  | $B_0$   | $A_1$   | $B_1$    | $A_2$    | $B_2$     |
|---|--------|---------|---------|----------|----------|-----------|
| $4s_{1/2} \rightarrow 3d_{5/2}(m = +1/2)$ | 5.8656 | 1.4073  | 67.7703 | 15.9049  | 922.6884 | 215.8052  |
| $4s_{1/2} \rightarrow 3d_{5/2}(m = +3/2)$ | 5.8656 | 0.3518  | 67.7703 | 3.9762   | 922.6884 | 53.9513   |
| $4s_{1/2} \rightarrow 3d_{5/2}(m = +5/2)$ | 5.8656 | -1.7591 | 67.7703 | -19.8812 | 922.6884 | -269.7565 |

where the transitions of  $3d_{5/2} \rightarrow nl$  include the  $3d_{5/2} \rightarrow np_{3/2}(n \geq 5)$  and  $3d_{5/2} \rightarrow nf_{5/2,7/2}(n \geq 4)$  transitions.  $C_n$  is written as

$$C_n = (-1)^{j_i+j_n} \frac{3m_j^2 - j_i(j_i+1)}{j_i(2j_i-1)} \begin{Bmatrix} 1 & 1 & 2 \\ j_i & j_i & j_n \end{Bmatrix} \sqrt{\frac{30j_i(2j_i-1)(2j_i+1)}{(j_i+1)(2j_i+3)}}. \quad (16)$$

In Eq. (15), because the  $\omega$  is the frequency of the longest magic wavelength,  $\frac{\omega}{\Delta E_{3d_{5/2} \rightarrow nl}}$  and  $\frac{\omega}{\Delta E_{4s_{1/2} \rightarrow np_j}}$  are less than 1.  $G(\omega, \cos^2 \theta_p)$  can be expanded as

$$G(\omega, \cos^2 \theta_p) = \sum_{k=0}^{\infty} \left[ A_k + \frac{3 \cos^2 \theta_p - 1}{2} B_k \right] \omega^{2k}, \quad (17)$$

in which the Taylor-series expansion is used, and  $A_k$  and  $B_k$  are written as

$$A_k = \sum_n \frac{f_{3d_{5/2} \rightarrow nl}}{\Delta E_{3d_{5/2} \rightarrow nl}^{2+2k}} - \sum_{n=5}^{\infty} \frac{f_{4s_{1/2} \rightarrow np_j}}{\Delta E_{4s_{1/2} \rightarrow np_j}^{2+2k}} \quad (18)$$

and

$$B_k = \sum_n C_n \times \frac{f_{3d_{5/2} \rightarrow nl}}{\Delta E_{3d_{5/2} \rightarrow nl}^{2+2k}}. \quad (19)$$

It can be seen that  $A_0$  is the difference in the static polarizabilities of the  $4s_{1/2}$  and  $3d_{5/2}$  states, excluding the contributions of the  $4s_{1/2} \rightarrow 4p_{1/2}$  and  $4s_{1/2} \rightarrow 4p_{3/2}$  transitions to the  $4s_{1/2}$  state and the  $3d_{5/2} \rightarrow 4p_{3/2}$  transition to the  $3d_{5/2}$  state.  $B_0$  is the contribution of the static tensor polarizabilities to the static polarizability for each of the  $3d_{5/2}$  magnetic states, excluding the contribution of the  $3d_{5/2} \rightarrow 4p_{3/2}$  transition. Table II lists the present calculations of  $A_0$ ,  $B_0$ ,  $A_1$ ,  $B_1$ ,  $A_2$ , and  $B_2$ .  $A_k$  and  $B_k$  ( $k \geq 3$ ) are not given because they contribute less than  $10^{-5}$  to  $G(\omega, \cos^2 \theta_p)$ . The present  $A_0$ , 5.866, agrees with the relativistic all-order single-double method result 5.928 [24] very well. The difference is about 1%. According to Eq. (12), the oscillator strength of the  $3d_{5/2} \rightarrow 4p_{3/2}$  transition becomes

$$f_{3d_{5/2} \rightarrow 4p_{3/2}} = \left( \frac{f_{4s_{1/2} \rightarrow 4p_{1/2}}}{\Delta E_{4s_{1/2} \rightarrow 4p_{1/2}}^2 - \omega^2} + \frac{f_{4s_{1/2} \rightarrow 4p_{3/2}}}{\Delta E_{4s_{1/2} \rightarrow 4p_{3/2}}^2 - \omega^2} - G(\omega, \cos^2 \theta_p) \right) \times \frac{\Delta E_{3d_{5/2} \rightarrow 4p_{3/2}}^2 - \omega^2}{C}. \quad (20)$$

In this equation, the transition energies  $\Delta E_{4s_{1/2} \rightarrow 4p_{1/2}}$ ,  $\Delta E_{4s_{1/2} \rightarrow 4p_{3/2}}$ , and  $\Delta E_{3d_{5/2} \rightarrow 4p_{3/2}}$  and the oscillator strengths  $f_{4s_{1/2} \rightarrow 4p_{1/2}}$  and  $f_{4s_{1/2} \rightarrow 4p_{3/2}}$  have been determined in the other experiments [15,42]. Therefore, we suggest that the high-precision measurements of the longest magic wavelength for the  $4s_{1/2} \rightarrow 3d_{5/2}$  transition can be used to determine the oscillator strength of the  $3d_{5/2} \rightarrow 4p_{3/2}$  transition.

It should be noted in Eq. (20) that the accuracy of  $f_{3d_{5/2} \rightarrow 4p_{3/2}}$  determined by measuring the longest magic wavelength is related to four factors. The first factor is the accuracy of the transition energy. The experimental energies (in hartrees) from the National Institute of Science and Technology (NIST) are correct to seven significant digits [42]. Therefore, this factor on the accuracy of  $f_{3d_{5/2} \rightarrow 4p_{3/2}}$  can be ignored. The second factor is the accuracy of  $f_{4s_{1/2} \rightarrow 4p_{1/2}}$  and  $f_{4s_{1/2} \rightarrow 4p_{3/2}}$ . As far as we know, the most accurate  $f_{4s_{1/2} \rightarrow 4p_{3/2}}$  is 0.682 [42], and the oscillator strength ratio of  $f_{4s_{1/2} \rightarrow 4p_{3/2}} : f_{4s_{1/2} \rightarrow 4p_{1/2}}$  is 2.027(5) [15]. We have estimated the uncertainty of  $f_{3d_{5/2} \rightarrow 4p_{3/2}}$  using these two values. We found that the uncertainty of  $f_{3d_{5/2} \rightarrow 4p_{3/2}}$  is within 0.6%. The third factor

is the accuracy of frequency  $\omega$  and angle  $\theta_p$  measurement. We found that the uncertainty of  $f_{3d_{5/2} \rightarrow 4p_{3/2}}$  does not exceed 0.06% when the angle  $\theta_p$  has 1 deg of error. And if the magic wavelengths have 0.01 nm error, it will lead to 0.02% uncertainty for  $f_{3d_{5/2} \rightarrow 4p_{3/2}}$ . So, this factor is also very small with regard to the uncertainty of  $f_{3d_{5/2} \rightarrow 4p_{3/2}}$ . The fourth factor is the accuracy of  $G(\omega, \cos^2 \theta_p)$ . The value of  $G(\omega, \cos^2 \theta_p)$  is dominated by the first terms  $A_0$  and  $B_0$ , which contribute more than 98%. Moreover, as mentioned before, the present  $A_0$  and  $B_0$  are in good agreement with the calculation of Arora *et al.* [24], and the difference is about 1%. Changing the value of  $G(\omega, \cos^2 \theta_p)$  by 5% (over estimated) leads to  $f_{3d_{5/2} \rightarrow 4p_{3/2}}$  changing by 0.3%. Therefore, taking all factors together, the uncertainty of  $f_{3d_{5/2} \rightarrow 4p_{3/2}}$  determined by measuring the longest magic wavelength does not exceed 1%.

In the above, only the  $f_{3d_{5/2} \rightarrow 4p_{3/2}}$  is determined by measuring the longest magic wavelength at any one angle for the  $4s_{1/2} \rightarrow 3d_{5/2}$  transition. As shown in Eq. (12), if the three longest magic wavelengths are measured at three different angles, the  $f_{4s_{1/2} \rightarrow 4p_{1/2}}$ ,  $f_{4s_{1/2} \rightarrow 4p_{3/2}}$ , and  $f_{3d_{5/2} \rightarrow 4p_{3/2}}$  will be determined

simultaneously. We also have estimated the uncertainties of these three oscillator strengths. The accuracies of  $f_{4s \rightarrow 4p_{1/2}}$  and  $f_{4s \rightarrow 4p_{3/2}}$  are very sensitive to the accuracy of  $\omega$ . If the errors of the magic wavelengths are 0.001 nm, it will lead to 5%, 3%, and 0.1% uncertainties for  $f_{4s \rightarrow 4p_{1/2}}$ ,  $f_{4s \rightarrow 4p_{3/2}}$ , and  $f_{3d_{5/2} \rightarrow 4p_{3/2}}$ , respectively. Changing the value of  $G(\omega, \cos^2 \theta_p)$  by 5% leads to  $f_{4s \rightarrow 4p_{1/2}}$ ,  $f_{4s \rightarrow 4p_{3/2}}$ , and  $f_{3d_{5/2} \rightarrow 4p_{3/2}}$  changing by 5%. In order to get high-precision oscillator strengths, the errors of the magic wavelengths should be smaller than 0.0001 nm and the uncertainty of  $G(\omega, \cos^2 \theta_p)$  should be smaller than 1%.

Combining the oscillator strength  $f_{4s \rightarrow 4p_{3/2}} = 0.682$  [42],  $f_{4s_{1/2} \rightarrow 4p_{3/2}} : f_{4s \rightarrow 4p_{1/2}} = 2.027(5)$  [15], and  $A_1$ ,  $A_2$ ,  $B_1$ , and  $B_2$  in Table II, as can be seen from Eqs. (12) and (17), the  $f_{3d_{5/2} \rightarrow 4p_{3/2}}$ ,  $A_0$ , and  $B_0$  can also be determined simultaneously using three magic wavelengths which are measured at three different angles. By using the uncertainties of  $f_{4s \rightarrow 4p_{1/2}}$  and  $f_{4s_{1/2} \rightarrow 4p_{3/2}} : f_{4s \rightarrow 4p_{1/2}}$ , we obtained that the uncertainties of  $f_{3d_{5/2} \rightarrow 4p_{3/2}}$ ,  $A_0$ , and  $B_0$  are 1%. If the errors of the magic wavelengths are 0.001 nm, the uncertainties of  $f_{3d_{5/2} \rightarrow 4p_{3/2}}$ ,  $A_0$ , and  $B_0$  will be 0.7%, 3.6%, and 9%, respectively. When the errors of the magic wavelengths are improved to 0.0001 nm, the uncertainties of  $f_{3d_{5/2} \rightarrow 4p_{3/2}}$ ,  $A_0$ , and  $B_0$  will be reduced to 0.1%, 0.4%, and 1%, respectively. That means the accuracies of  $A_0$  and  $B_0$  are very sensitive to the accuracy of the magic wavelength. In order to get the values of  $A_0$  and  $B_0$  with a very high degree of precision, the high-precision magic wavelengths are required.

In principle, if the five longest magic wavelengths can be measured at five different angles, the five parameters,  $f_{4s \rightarrow 4p_{1/2}}$ ,  $f_{4s \rightarrow 4p_{3/2}}$ ,  $f_{3d_{5/2} \rightarrow 4p_{3/2}}$ ,  $A_0$ , and  $B_0$ , would be determined simultaneously. The uncertainties of these five parameters will depend on the accuracies of  $A_k$  and  $B_k$  ( $k \geq 1$ ). However, at present, the accuracies of  $A_k$  and  $B_k$  ( $k \geq 1$ ) cannot be guaranteed to be smaller than 5%. So, the determination of these five parameters by using five magic wavelengths is not a good choice.

### B. Magic wavelengths for the $4s_{1/2} \rightarrow 3d_{3/2}$ transition

Three magic wavelengths are found for each of the  $4s_{1/2} \rightarrow 3d_{3/2}$  magnetic sublevel transitions. Figure 5 shows the dependence of the magic wavelengths for each of the  $4s_{1/2} \rightarrow 3d_{3/2}$  magnetic transitions upon  $\cos^2 \theta_p$ . Similarly, the magic wavelength near 395.79 nm is insensitive to  $\cos^2 \theta_p$ , while the longest magic wavelength, which is longer than the  $3d_{3/2} \rightarrow 4p_{1/2}$  transition wavelength 866.21 nm, strongly depends on  $\cos^2 \theta_p$ .

A similar behavior occurs also for the longest magic wavelengths of the  $4s_{1/2} \rightarrow 3d_{3/2}$  transition with those of the  $4s_{1/2} \rightarrow 3d_{5/2}$  transition. At the longest magic wavelength, the oscillator strengths,  $f_{3d_{3/2} \rightarrow 4p_{1/2}}$  and  $f_{3d_{3/2} \rightarrow 4p_{3/2}}$ , satisfy the following equation:

$$\frac{f_{4s_{1/2} \rightarrow 4p_{1/2}}}{\Delta E_{4s \rightarrow 4p_{1/2}}^2 - \omega^2} + \frac{f_{4s \rightarrow 4p_{3/2}}}{\Delta E_{4s \rightarrow 4p_{3/2}}^2 - \omega^2} - \frac{C_1 f_{3d_{3/2} \rightarrow 4p_{1/2}}}{\Delta E_{3d_{3/2} \rightarrow 4p_{1/2}}^2 - \omega^2} - \frac{C_2 f_{3d_{3/2} \rightarrow 4p_{3/2}}}{\Delta E_{3d_{3/2} \rightarrow 4p_{3/2}}^2 - \omega^2} = G'(\omega, \cos^2 \theta_p). \quad (21)$$

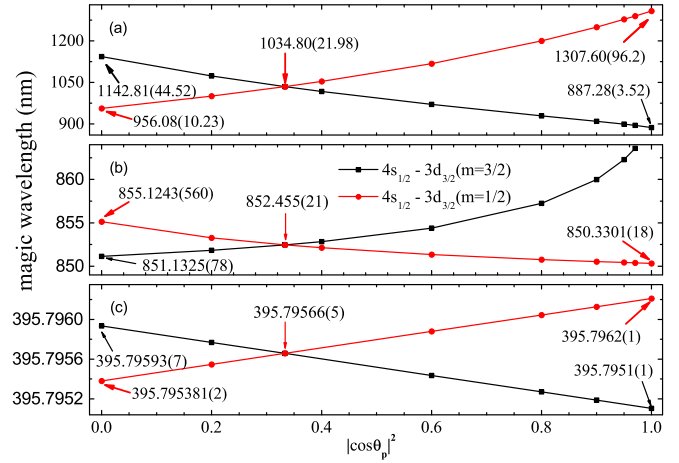


FIG. 5. Magic wavelengths of the  $4s_{1/2} \rightarrow 3d_{3/2}$  transition of the  $\text{Ca}^+$  ions for linearly polarized light. (a) Magic wavelengths longer than the  $3d_{3/2} \rightarrow 4p_{1/2}$  transition wavelength (866.21 nm). (b) Magic wavelengths which lie between the  $3d_{3/2} \rightarrow 4p_{3/2}$  transition wavelength (849.80 nm) and the  $3d_{3/2} \rightarrow 4p_{1/2}$  transition wavelength (866.21 nm). (c) Magic wavelengths which lie between the  $4s_{1/2} \rightarrow 4p_{1/2}$  transition wavelength (393.37 nm) and the  $4s_{1/2} \rightarrow 4p_{3/2}$  transition wavelength (396.85 nm).

$G'(\omega, \cos^2 \theta_p)$  is defined as

$$G'(\omega, \cos^2 \theta_p) = \alpha_{3d_{3/2}}^R(\omega, \cos^2 \theta_p) - \alpha_{4s_{1/2}}^R(\omega), \quad (22)$$

where  $\alpha_{3d_{3/2}}^R(\omega, \cos^2 \theta_p)$  is the dynamic polarizability of the  $3d_{3/2}$  state, excluding the contributions from the  $3d_{3/2} \rightarrow 4p_{1/2}$  and  $3d_{3/2} \rightarrow 4p_{3/2}$  transitions.  $C_1$  and  $C_2$  can be written as

$$C_1 = 1 + \frac{3 \cos^2 \theta_p - 1}{2} \left( \frac{5}{4} - m_{j_i}^2 \right) \quad (23)$$

and

$$C_2 = 1 + \frac{3 \cos^2 \theta_p - 1}{2} \left( \frac{4}{5} m_{j_i}^2 - 1 \right), \quad (24)$$

where  $m_{j_i}$  is magnetic quantum number of the  $3d_{3/2}$  state.  $G'(\omega, \cos^2 \theta_p)$  can also be simplified by using Taylor-series expansion. The expanded form is similar to Eqs. (17)–(19), except that the  $3d_{5/2}$  state is replaced by the  $3d_{3/2}$  state.

Table III lists the values of  $A_0$ ,  $B_0$ ,  $A_1$ ,  $B_1$ ,  $A_2$ , and  $B_2$  for the  $4s_{1/2} \rightarrow 3d_{3/2}$   $m = 1/2, 3/2$  transitions, respectively.

TABLE III. Values of parameters  $A_k$  and  $B_k$  ( $k = 0, 1, 2$ ) for each of the  $4s_{1/2} \rightarrow 3d_{3/2}$  magnetic sublevel transitions.  $m$  is the magnetic quantum number of the  $3d_{3/2}$  state.

|       | $4s_{1/2} \rightarrow 3d_{3/2}$ |           |
|-------|---------------------------------|-----------|
|       | $m = 1/2$                       | $m = 3/2$ |
| $A_0$ | 5.8321                          | 5.8321    |
| $B_0$ | 1.2233                          | -1.2233   |
| $A_1$ | 67.1954                         | 67.1954   |
| $B_1$ | 13.7798                         | -13.7798  |
| $A_2$ | 912.4437                        | 912.4437  |
| $B_2$ | 186.3584                        | -186.3584 |

Since the transition energies  $\Delta E_{4s_{1/2} \rightarrow 4p_{1/2}}$ ,  $\Delta E_{4s_{1/2} \rightarrow 4p_{3/2}}$ ,  $\Delta E_{3d_{3/2} \rightarrow 4p_{1/2}}$ , and  $\Delta E_{3d_{3/2} \rightarrow 4p_{3/2}}$  and the oscillator strengths  $f_{4s_{1/2} \rightarrow 4p_{1/2}}$  and  $f_{4s_{1/2} \rightarrow 4p_{3/2}}$  are known (as mentioned before), using Eq. (21) the oscillator strengths for the  $3d_{3/2} \rightarrow 4p_{1/2}$  and  $3d_{3/2} \rightarrow 4p_{3/2}$  transitions can be determined by measurement of the two longest magic wavelengths of the  $4s_{1/2} \rightarrow 3d_{3/2}$  transition at two different angles.

It should be noted that the uncertainties of  $f_{3d_{3/2} \rightarrow 4p_{1/2}}$  and  $f_{3d_{3/2} \rightarrow 4p_{3/2}}$ , determined by measurement of the magic wavelength, depend on the accuracies of  $f_{4s_{1/2} \rightarrow 4p_{1/2}}$ ,  $f_{4s_{1/2} \rightarrow 4p_{3/2}}$ ,  $\omega$ , and  $G'(\omega, \cos^2 \theta_p)$ . We found that the accuracies of  $f_{3d_{3/2} \rightarrow 4p_{1/2}}$  and  $f_{3d_{3/2} \rightarrow 4p_{3/2}}$  are identical with the accuracies of  $f_{4s_{1/2} \rightarrow 4p_{1/2}}$  and  $f_{4s_{1/2} \rightarrow 4p_{3/2}}$ . The uncertainties of  $f_{3d_{3/2} \rightarrow 4p_{1/2}}$  and  $f_{3d_{3/2} \rightarrow 4p_{3/2}}$  are smaller than 1% when the value of  $G'(\omega, \cos^2 \theta_p)$  has 5% uncertainty. If the magic wavelengths have 0.001 nm errors, the uncertainties of  $f_{3d_{3/2} \rightarrow 4p_{1/2}}$  and  $f_{3d_{3/2} \rightarrow 4p_{3/2}}$  will be 0.01% and 0.08%. Therefore, we suggest that the measurement of the longest magic wavelengths for the  $4s_{1/2} \rightarrow 3d_{3/2}$  transition at any two angles can be used to determine  $f_{3d_{3/2} \rightarrow 4p_{1/2}}$  and  $f_{3d_{3/2} \rightarrow 4p_{3/2}}$ , and the uncertainties of  $f_{3d_{3/2} \rightarrow 4p_{1/2}}$  and  $f_{3d_{3/2} \rightarrow 4p_{3/2}}$  are smaller than 2%.

#### IV. CONCLUSIONS

The dynamic polarizabilities of the  $4s_{1/2}$  and  $3d_j$  states of the  $\text{Ca}^+$  ions are calculated. The magic wavelengths for the  $4s_{1/2} \rightarrow 3d_{3/2,5/2}$  transitions are identified for  $\hat{e}_z \perp \hat{\epsilon}$  and  $\hat{e}_z \parallel \hat{\epsilon}$  in the case of linearly polarized light ( $\cos \theta_k = 0$  or  $\mathcal{A} = 0$ ). The dependence of the magic wavelengths upon  $\cos^2 \theta_p$  is analyzed. It is found that the magic wavelength near 395.79 nm is insensitive to the angle between the quantization axis  $\hat{e}_z$  and the polarization vector  $\hat{\epsilon}$ . In contrast, the longest magic wavelength which is longer than the  $3d_{5/2} \rightarrow 4p_{3/2}$  transition wavelength (854.21 nm) is very sensitive to  $\cos^2 \theta_p$ .

We suggest that accurate measurements on the longest magic wavelengths for the  $4s_{1/2} \rightarrow 3d_{5/2}$  transition can be used to determine the oscillator strength of the  $3d_{5/2} \rightarrow 4p_{3/2}$  transition and the uncertainty will be smaller than 1%. If the three longest magic wavelengths are measured with errors smaller than 0.0001 nm, oscillator strengths of the  $4s_{1/2} \rightarrow 4p_{1/2}$  and  $4s_{1/2} \rightarrow 4p_{3/2}$  transitions will be determined with a very high accuracy.

Combining the oscillator strength  $f_{4s_{1/2} \rightarrow 4p_{3/2}} = 0.682$  [42] and  $f_{4s_{1/2} \rightarrow 4p_{3/2}} : f_{4s_{1/2} \rightarrow 4p_{1/2}} = 2.027(5)$  [15], the difference in the static polarizabilities for the  $4s_{1/2}$  and  $3d_{5/2}$  states can also be determined simultaneously by using the three longest magic wavelengths for the  $4s_{1/2} \rightarrow 3d_{5/2}$  transition, which are measured at three different angles. The difference in the static polarizabilities for  $4s_{1/2}$  and  $3d_{5/2}$  is very important for the estimation of blackbody radiation shift of the  $\text{Ca}^+$  ion clock.

The measurement of the longest magic wavelengths for the  $4s_{1/2} \rightarrow 3d_{3/2}$  transition at any two angles can be used to determine  $f_{3d_{3/2} \rightarrow 4p_{1/2}}$  and  $f_{3d_{3/2} \rightarrow 4p_{3/2}}$ , and the uncertainties of  $f_{3d_{3/2} \rightarrow 4p_{1/2}}$  and  $f_{3d_{3/2} \rightarrow 4p_{3/2}}$  will be smaller than 2%.

The present suggestion of using the measurements of the longest angle-dependent magic wavelengths to determine oscillator strengths and other atomic parameters for  $\text{Ca}^+$  can also be applied to  $\text{Be}^+$ ,  $\text{Mg}^+$ ,  $\text{Sr}^+$ ,  $\text{Ba}^+$  ions and some neutral alkali-metal atoms.

#### ACKNOWLEDGMENTS

This work is supported by the National Key Research and Development Program of China under Grant No. 2017YFA0402300, the National Natural Science Foundation of China (NSFC) (Grants No. 11564036, No. 11774292, No. 11864036, and No. 11804280), and the Young Teachers Scientific Research Ability Promotion Plan of Northwest Normal University (Grant No. NWNLU-LKQN-15-3).

- 
- [1] T. G. Tiecke, J. D. Thompson, N. P. de Leon, L. R. Liu, V. Vuletić, and M. D. Lukin, *Nature (London)* **508**, 241 (2014).
- [2] H. Häffner, C. Roos, and R. Blatt, *Phys. Rep.* **469**, 155 (2008).
- [3] G. Wilpers, C. W. Oates, S. A. Diddams, A. Bartels, T. M. Fortier, W. H. Oskay, J. C. Bergquist, S. R. Jefferts, T. P. Heavner, T. E. Parker, and L. Hollberg, *Metrologia* **44**, 146 (2007).
- [4] C. Monroe, D. M. Meekhof, B. E. King, W. M. Itano, and D. J. Wineland, *Phys. Rev. Lett.* **75**, 4714 (1995).
- [5] S. N. Lea, *Rep. Prog. Phys.* **70**, 1473 (2007).
- [6] C. S. Wood, S. C. Bennett, D. Cho, B. P. Masterson, J. L. Roberts, C. E. Tanner, and C. E. Wieman, *Science* **275**, 1759 (1997).
- [7] A. D. Ludlow, T. Zelevinsky, G. K. Campbell, S. Blatt, M. M. Boyd, M. H. G. de Miranda, M. J. Martin, J. W. Thomsen, S. M. Foreman, J. Ye, T. M. Fortier, J. E. Stalnaker, S. A. Diddams, Y. Le Coq, Z. W. Barber, N. Poli, N. D. Lemke, K. M. Beck, and C. W. Oates, *Science* **319**, 1805 (2008).
- [8] T. Rosenband, D. B. Hume, P. O. Schmidt, C. W. Chou, A. Brusch, L. Lorini, W. H. Oskay, R. E. Drullinger, T. M. Fortier, J. E. Stalnaker, S. A. Diddams, W. C. Swann, N. R. Newbury, W. M. Itano, D. J. Wineland, and J. C. Bergquist, *Science* **319**, 1808 (2008).
- [9] N. Hinkley, J. A. Sherman, N. B. Phillips, M. Schioppa, N. D. Lemke, K. Beloy, M. Pizzocaro, C. W. Oates, and A. D. Ludlow, *Science* **341**, 1215 (2013).
- [10] Y. Huang, J. Cao, P. Liu, K. Liang, B. Ou, H. Guan, X. Huang, T. Li, and K. Gao, *Phys. Rev. A* **85**, 030503 (2012).
- [11] M. Takamoto, F.-L. Hong, R. Higashi, and H. Katori, *Nature (London)* **435**, 321 (2005).
- [12] Y. Huang, H. Guan, P. Liu, W. Bian, L. Ma, K. Liang, T. Li, and K. Gao, *Phys. Rev. Lett.* **116**, 013001 (2016).
- [13] J. Ye, D. W. Vernooy, and H. J. Kimble, *Phys. Rev. Lett.* **83**, 4987 (1999).
- [14] H. Katori, T. Ido, and M. K. Gonokami, *J. Phys. Soc. Jpn.* **68**, 2479 (1999).
- [15] P.-L. Liu, Y. Huang, W. Bian, H. Shao, H. Guan, Y.-B. Tang, C.-B. Li, J. Mitroy, and K.-L. Gao, *Phys. Rev. Lett.* **114**, 223001 (2015).
- [16] J. H. Becher, S. Baier, K. Aikawa, M. Lepers, J.-F. Wyatt, O. Dulieu, and F. Ferlaino, *Phys. Rev. A* **97**, 012509 (2018).

- [17] N. L. Manakov, V. D. Ovsiannikov, and L. P. Rapoport, *Phys. Rep.* **141**, 320 (1986).
- [18] K. Beloy, Theory of the ac Stark Effect on the Atomic Hyperfine Structure and Applications to Microwave Atomic Clocks, Ph.D. thesis, University of Nevada, 2009.
- [19] M. Chwalla, J. Benhelm, K. Kim, G. Kirchmair, T. Monz, M. Riebe, P. Schindler, A. S. Villar, W. Hänsel, C. F. Roos, R. Blatt, M. Abgrall, G. Santarelli, G. D. Rovera, and P. Laurent, *Phys. Rev. Lett.* **102**, 023002 (2009).
- [20] K. Matsubara, H. Hachisu, Y. Li, S. Nagano, C. Locke, A. Nogami, M. Kajita, K. Hayasaka, T. Ido, and M. Hosokawa, *Opt. Express* **20**, 22034 (2012).
- [21] H. C. Nägerl, C. Roos, D. Leibfried, H. Rohde, G. Thalhammer, J. Eschner, F. Schmidt-Kaler, and R. Blatt, *Phys. Rev. A* **61**, 023405 (2000).
- [22] A. Kreuter, C. Becher, G. P. T. Lancaster, A. B. Mundt, C. Russo, H. Häffner, C. Roos, W. Hänsel, F. Schmidt-Kaler, R. Blatt, and M. S. Safronova, *Phys. Rev. A* **71**, 032504 (2005).
- [23] P. A. Barton, C. J. S. Donald, D. M. Lucas, D. A. Stevens, A. M. Steane, and D. N. Stacey, *Phys. Rev. A* **62**, 032503 (2000).
- [24] B. Arora, M. S. Safronova, and C. W. Clark, *Phys. Rev. A* **76**, 064501 (2007).
- [25] C. Champenois, M. Houssin, C. Lisowski, M. Knoop, G. Hagel, M. Vedel, and F. Vedel, *Phys. Lett. A* **331**, 298 (2004).
- [26] M. Kajita, Y. Li, K. Matsubara, K. Hayasaka, and M. Hosokawa, *Phys. Rev. A* **72**, 043404 (2005).
- [27] Y.-B. Tang, H.-X. Qiao, T.-Y. Shi, and J. Mitroy, *Phys. Rev. A* **87**, 042517 (2013).
- [28] J. Kaur, S. Singh, B. Arora, and B. K. Sahoo, *Phys. Rev. A* **92**, 031402 (2015).
- [29] D. L. Haycock, S. E. Hamann, G. Klose, and P. S. Jessen, *Phys. Rev. A* **55**, R3991 (1997).
- [30] T. A. Savard, K. M. O'Hara, and J. E. Thomas, *Phys. Rev. A* **56**, 1095(R) (1997).
- [31] C. D. Herold, V. D. Vaidya, X. Li, S. L. Rolston, J. V. Porto, and M. S. Safronova, *Phys. Rev. Lett.* **109**, 243003 (2012).
- [32] R. H. Leonard, A. J. Fallon, C. A. Sackett, and M. S. Safronova, *Phys. Rev. A* **92**, 052501 (2015).
- [33] A. Fallon and C. Sackett, *Atoms* **4**, 12 (2016).
- [34] W. F. Holmgren, R. Trubko, I. Hromada, and A. D. Cronin, *Phys. Rev. Lett.* **109**, 243004 (2012).
- [35] R. Trubko, M. D. Gregoire, W. F. Holmgren, and A. D. Cronin, *Phys. Rev. A* **95**, 052507 (2017).
- [36] M. S. Safronova, Z. Zuhrianda, U. I. Safronova, and C. W. Clark, *Phys. Rev. A* **92**, 040501 (2015).
- [37] J. Jiang, L.-Y. Tang, and J. Mitroy, *Phys. Rev. A* **87**, 032518 (2013).
- [38] J. Jiang, J. Mitroy, Y. Cheng, and M. W. J. Bromley, *Phys. Rev. A* **94**, 062514 (2016).
- [39] J. Jiang, L. Jiang, X. Wang, D.-H. Zhang, L.-Y. Xie, and C.-Z. Dong, *Phys. Rev. A* **96**, 042503 (2017).
- [40] F. Le Kien, P. Schneeweiss, and A. Rauschenbeutel, *Eur. Phys. J. D* **67**, 92 (2013).
- [41] D. Budker, D. F. Kimball, and D. P. DeMille, *Atomic Physics: An Exploration Through Problems and Solutions* (Oxford University Press, Oxford, England, 2004).
- [42] A. Kramida, Y. Ralchenko, J. Reader, and NIST ASD Team, NIST Atomic Spectra Database (ver. 5.6.1), [Online]; Available: <https://physics.nist.gov/asd> [2018, December 12], National Institute of Standards and Technology, Gaithersburg, MD (2018).